UC San Diego

UC San Diego Previously Published Works

Title

Vitamin E functions by association with a novel binding site on the 67 kDa laminin receptor activating diacylglycerol kinase.

Permalink

https://escholarship.org/uc/item/71g5t9g7

Authors

Shirai, Yasuhito
Hayashi, Daiki
Mouchlis, Varnavas
et al.

Publication Date

2022-12-01

DOI

10.1016/j.jnutbio.2022.109129

Peer reviewed

eScholarship.org Powered by the California Digital Library
University of California

Author Manuscript

Author Manuscript

Author Manuscript

Author Manuscript

HHS Public Access

Author manuscript

J Nutr Biochem. Author manuscript; available in PMC 2023 December 01.

Published in final edited form as:

J Nutr Biochem. 2022 December ; 110: 109129. doi:10.1016/j.jnutbio.2022.109129.

Vitamin E Functions by Association with a Novel Binding Site on the 67 kDa Laminin Receptor Activating Diacylglycerol Kinase

Daiki Hayashi[1,2], **Varnavas D. Mouchlis**[2], **Seika Okamoto**[1], **Liuqing Wang**[1], **Sheng Li**[3], **Shuji Ueda**[1], **Minoru Yamanoue**[1], **Hirofumi Tachibana**[4], **Hiroyuki Arai**[5], **Hitoshi Ashida**[1], **Edward A. Dennis**[2], **Yasuhito Shirai**[1,*]

[1]Department of Applied Chemistry in Bioscience, Graduate School of Agricultural Science, Faculty of Agriculture, Kobe University, Kobe 657-8501, Japan

[2]Department of Pharmacology, and Department of Chemistry and Biochemistry, University of California San Diego, La Jolla, California 92093, USA

[3]Department of Medicine, University of California San Diego, La Jolla, California 92093, USA

[4]Division of Applied Biological Chemistry, Department of Bioscience and Biotechnology, Faculty of Agriculture, Kyushu University, Fukuoka, 819-0395, Japan

[5]Department of Health Chemistry, Graduate School of Pharmaceutical Sciences, University of Tokyo, Tokyo 113-0033, Japan

Abstract

It is generally recognized that the main function of α-tocopherol (αToc), which is the most active form of vitamin E, is its antioxidant effect, while non-antioxidant effects have also been reported. We previously found that αToc ameliorates diabetic nephropathy via diacylglycerol kinase alpha (DGKα) activation in vivo, and the activation was not related to the antioxidant effect. However, the underlying mechanism of how αToc activates DGKα have been enigmatic. We report that the membrane-bound 67 kDa laminin receptor (67LR), which has previously been shown to serve as a receptor for epigallocatechin gallate (EGCG), also contains a novel binding site for vitamin E, and its association with Vitamin E mediates DGKα activation by αToc. We employed hydrogen-deuterium exchange mass spectrometry (HDX/MS) and molecular dynamics (MD) simulations to identify the specific binding site of αToc on the 67LR and discovered the conformation of the specific hydrophobic pocket that accommodates αToc. Also, HDX/MS and MD simulations demonstrated the detailed binding of EGCG to a water-exposed hydrophilic site on 67LR, while in contrast αToc binds to a distinct hydrophobic site. We demonstrated that 67LR triggers an important signaling pathway mediating non-antioxidant effects of αToc, such as

[*]**Correspondence to** Yasuhito Shirai (shirai@kobe-u.ac.jp).

AUTHOR CONTRIBUTIONS

D. H. performed most of the experiments and analyzed most of the data. V. D. M. helped with HDX/MS and performed MD simulations. S. O. performed a mutant experiment. L. W. analyzed αToc by HPLC. S. L. analyzed the HDX/MS samples. H. T. and H. A. provided information about 67LR and α-TTP. S. U., M. Y. and H. A. advised on the experiments. E. A. D. advised on the HDX/MS and MD simulations. D. H., V. D. M., E. A. D., and Y. S. wrote the manuscript. D. H., V. D. M., and Y. S. conceived the project. Y. S. supervised the research.

SUPPORTING INFORMATION

The Supporting Tables, Figures, and Movies are available online.

Author Manuscript Author Manuscript Author Manuscript Author Manuscript

DGKα activation. This is the first evidence demonstrating a membrane receptor for αToc and one of the underlying mechanisms of a non-antioxidant function for αToc.

Keywords

vitamin E; 67 kDa laminin receptor; diacylglycerol kinase; epigallocatechin gallate

INTRODUCTION

Tocopherols are hydrophobic antioxidant agents known generally as vitamin E. D-α-tocopherol (αToc) is the most active Vitamin E compound that humans preferentially absorb and accumulate [1]. The main function of αToc is recognized as its antioxidant effect preventing lipid peroxidation of polyunsaturated fatty acids (PUFAs) in the cell membrane [2], but many other functions, such as activation of signal transduction and gene expression, that are not related to the antioxidant effect, have been reported [3]. For example, it has been suggested that αToc promotes drug-metabolizing gene expression via the nuclear receptor pregnane X receptor (PXR) [4]. Also, it has been reported that αToc inhibits the activity of protein kinase C [5]. Vitamin E was discovered in 1922 as an essential food component, but the specific target for vitamin E that mediates the non-antioxidant effect is still enigmatic. As a specific αToc binding protein, α-tocopherol transfer protein (α-TTP) plays a critical role in the transport of αToc in the liver, and deficiency of α-TTP causes ataxia with vitamin E deficiency (AVED) [6–8]. However, a cell membrane receptor for αToc, which mediates specific signal transduction, has not been reported.

Koya *et al.* [9] reported that αToc ameliorated the symptoms of diabetic nephropathy (DN) by inhibiting diabetes-induced abnormal protein kinase C (PKC) activation in glomerulus through activation of a lipid kinase: diacylglycerol kinase (DGK). We have reported that αToc activates DGKα and that αToc ameliorated DN via DGKα in vivo [10–12]. Note that acetated αToc, which lacks antioxidant effect induces DGKα activation indicating the DGKα activation is a non- antioxidant effect of αToc [10]. These facts suggested that the effect of αToc on DN involves the non-antioxidant effects of αToc. Furthermore, the involvement of a receptor for αToc in the αToc-induced DGKα activation was suggested since the activation was an indirect effect [10]. However, the identity of the specific receptor which mediates αToc signaling has not been reported.

The 67 kDa laminin receptor (67LR) is primally found as a non-integrin laminin receptor [13–15]. It has also been reported that the Sindbis virus and pathogenic prion protein are the ligands for the 67LR [16,17]. In addition to these ligands, epigallocatechin gallate (EGCG), one of the green tea polyphenols, is a ligand for 67LR [18]. Finally, the expression level of 67LR is upregulated in various cancer cells, and EGCG shows an anti-cancer effect through 67LR [19–23]. Recently, we have found that EGCG indirectly activates DGKα and that 67LR is involved in the activation [24]. Also, we reported that EGCG ameliorated DN through DGKα in vivo, similar to αToc [25]. Based on these facts, we hypothesized that αToc also activates DGKα through the 67LR and that 67LR functions as an αToc receptor mediating the αToc signaling. Therefore, we explored whether αToc activates

Author Manuscript Author Manuscript Author Manuscript Author Manuscript

DGKα directly through 67LR and the binding of αToc to 67LR by taking advantage of hydrogen-deuterium exchange mass spectrometry (HDX/MS) and molecular dynamics (MD) simulation approaches.

HDX/MS is a powerful structural approach that can determine the specific interactions between a protein and its ligands in solution [26,27]. With HDX/MS, one can determine where various ligands bind to the protein by determining the inhibition of hydrogen-deuterium exchange in specific peptides in the protein backbone in the presence of specific ligands. In this study, we employed HDX/MS to discover a novel αToc binding site and to confirm the EGCG binding site on 67LR. Moreover, we performed MD simulations to investigate the detailed binding mode and confirmed the identity of the binding site using several mutants of 67LR.

METHODS

Cell culture

The *Mesocricetus auratus* leiomyosarcoma cell line (DDT1-MF-2 cells), *Cercopithecus aethiops* kidney cell line (Cos7 cells), and *homo sapience* colorectal carcinoma cell line (HCT116 cells) were cultured in Dulbecco's modified Eagle medium (DMEM)-high glucose supplied 10% fetal bovine serum, penicillin (100 units/ml), streptomycin (100 mg/ml) and L-glutamine. The cells were maintained in a humidified atmosphere containing 5% CO_2 at 37°C.

Imaging of the DGKα translocation

The live imaging of the DGKα translocation was performed following our previous method [24]. In short, 1.0×10^5 DDT1-MF-2 cells were inoculated in a glass-bottom 35 mm dish and allowed to adhere for 24 h. The N-terminal GFP-tag conjugated DGKα encoding plasmid was transfected using FuGene® HD Transfection Reagent (Promega Corporation, Madison WI, USA). After 24 h of transfection, the medium was replaced with buffer (165 mM NaCl, 5 mM KCl, 1 mM $MgCl_2$, 1 mM $CaCl_2$, 5 mM HEPES, 10 mM Glucose) and stimulated with various concentrations of αToc, αToc derivatives, or EGCG. Cells were observed with a confocal scanning microscope FV-1000 (Olympus Corporation, Tokyo, Japan). When the N-terminal FLAG-tag conjugated 67LR or its mutants were overexpressed, each plasmid was mixed equally with GFP-DGKα encoding plasmid, and used the mixture for transfection. When the cells were pretreated with the 67LR antibody, 20 μg/μl of the 67LR polyclonal antibody (N2C3, Cat. # GTX113485, GeneTex, Inc., Irvine CA, USA) was added into media 2 h before stimulation, and the same volume of normal rabbit serum was used as a negative control. The siRNA of 67LR (Sequence: 5'-UUCGCCCUGAAAUUCCUCC-3' and 5'-GGAGGAAUUUCAGGGCGAA-3') was transfected 24 h before transfection of GFP-DGKα. The translocation rate was calculated as a percentage of cells with translocated GFP-DGKα among at least 60 cells that express GFP-DGKα.

Author Manuscript Author Manuscript Author Manuscript Author Manuscript

Binding assay of αToc to recombinant 67LR

The FLAG-67LR and FLAG-α-TTP were overexpressed in the Cos7 cells using an electroporation method described previously [24]. The recombinant FLAG-tagged proteins were precipitated by anti-FLAG tagged antibody conjugated resin. The resin was incubated with various concentrations of αToc contained phosphate-buffered saline (PBS) for 15 min. The resin was washed, and bound αToc was extracted using 300 μl of ethyl acetate/hexane (1/9 v/v). The solvent was dried with nitrogen gas, and the extract was dissolved in 50 μl of 100% methanol. The sample was analyzed by the HPLC system using a TSKgel ODS-120T 2.0×250 mm column (Tosoh Corporation, Tokyo, Japan), and the peak of αToc was detected by UV (excitation: 298 nm emission: 330 nm). The empty vector was used as a negative control.

Preparing tocopherol conjugated beads

The tocopherol conjugated beads were prepared using D-α-tocopherol succinate (αTos) and NH_2 beads (TAMAGAWA SEIKI Co., Ltd., Nagano, Japan) by following the supplier recommended procedure. In brief, 10 mM αTos, 10 mM N-hydroxysuccinimide, and 10 mM 1-(3-dimethylaminopropyl)-3-ethyl carbodiimide hydrochloride were mixed in N, N-dimethylformamide (DMF) and activated by incubating for 2 h at 25°C. The 2.5 mg of NH_2 beads was incubated with 500 μl of activated ligand in solution for 16 h at 25°C. Finally, the beads were washed with DMF and incubated with 500 μl of 20% acetic anhydride in DMF to mask the remaining NH_2 moiety of the beads for 2 h at 25°C. The beads were washed and stored in H_2O at 4°C until use. The control beads were prepared with the same procedures without αTos.

Binding assay using tocopherol conjugated beads

The FLAG-67LR overexpressing Cos7 cell lysate was incubated with 0.5 mg of the tocopherol conjugated beads for 2 h at 4°C. The beads were washed with PBS containing 0.03% Triton X three times. The FLAG-67LR bound to tocopherol beads was detected by western blot using an anti-FLAG antibody for the primary antibody. The intensity of the bands was analyzed by Image J software.

Differential scanning fluorometry (DSF)

The N terminal GST and C terminal 6×His tag conjugated 67LR was purified using glutathione sepharose as describe following section. The mixture containing 10 or 100 μM of EGCG and αToc, 10 μM of purified protein, and 2× SYPRO® Orange (Thermo Fisher Scientific Inc., Waltham MA, USA) in the buffer (25 mM HEPES, pH 7.5, 100 mM NaCl) was incubated for 30 min at 25°C. After the incubation, the sample was heated from 25 °C to 70 °C by 2 °C/min, and the fluorescence was scanned using CFX Connect (BioRad Laboratories, Inc., Hercules, CA, USA) every 30 sec.

Isothermal Titration Calorimetry (ITC)

The ITC experiment was performed using MicroCal iTC200. The 20 mM αToc stock solution in DMSO was dissolved in the buffer (25 mM HEPES, pH 7.5, 100 mM NaCl) by 1/1000 dilution (the final concentration was 20 μM) and loaded to sample cell. The 120

Author Manuscript Author Manuscript Author Manuscript Author Manuscript

μM purified recombinant GST-67LR-His protein was dialyzed against the same buffer with the αToc sample and loaded to the injection syringe. The same amount of DMSO with the αToc sample was added to the protein sample. The protein sample was injected into the sample cell by 19 individual injections of 1.75 μl sample with 250 sec initial delay and 180 sec spacing time. The titration was performed at 25 °C (298K), and the sample cell was stirred by 750 rpm to ensure thorough mixing during the titration. The data were processed using Origin software, and K_d values were calculated. The experiments were performed three times using two independent batches of a protein sample, and representative data was shown as the final figure. The control experiments were performed by injecting the buffer to the αToc sample in the cell and the protein sample to the buffer in the cell to measure the heat of dilution.

Construction of 67LR mutants

The N-terminal FLAG-tagged 67LR mutants were constructed by the long PCR method using a FLAG-67LR plasmid that was prepared previously [24] as a template. The plasmid was amplified with respective primers shown in Table S1. The amplified products were transfected into DH5α *E. coli*. Several single colonies were picked, and the plasmid was purified to confirm the mutation using a restriction enzyme. Finally, the mutations were confirmed by DNA sequencing.

Molecular docking.

The 3D structure of the 67LR receptor (PDB ID: 3BCH) [28] was prepared using the Protein Preparation Wizard [29,30]. The 3D structures of αToc and EGCG were sketched using Maestro sketcher, and they were optimized using the LigPrep [30,31]. The box center for the docking calculations was defined using the centroid of selected residues that were found to constitute the EGCG binding site [18]. The grid required for the docking procedure was generated using a scaling factor of 1.0 and a partial charge cutoff of 0.25, while the X, Y, Z dimensions of the inner box were set to 12 Å. For the ligand docking, a scaling factor of 0.8 and partial charge cutoff of 0.15 were used to allow complete flexibility of the structures. The poses were selected according to the binding mode and the XP GScore. The Glide Extra-Precision (XP) scoring function was used for the calculations [32,33].

Expression and purification of recombinant 67LR

Recombinant 67LR protein was prepared by a bacterial expression system using *E. coli*. N-terminal GST tagged and C-terminal 6×His tagged conjugated 67LR encoding plasmid was transfected into BL21 *E. coli*. The *E. coli* were pre-cultured for 16 h at 37°C, and 20 ml of pre-cultured *E. coli* was cultured in 1 L of LB medium until the OD_{600} reached 0.7~1.0. The expression was induced with 0.2 mM of IPTG for 6 h at 25°C. The *E. coli* was harvested and lysed in lysis buffer (20 mM Tris-HCl pH 8.0, 1 mM EDTA, 1 mM DTT, 5 mM $MgCl_2$, 250 mM sucrose, 1 mM PMSF, 20 ng/ml leupeptin). The lysate was centrifuged, and the supernatant was subjected to purification using glutathione sepharose. The eluted protein sample was subjected to the DSF and the ITC experiment. For the HDX/MS experiment, the GST tag was removed by the following procedures. The elution fraction of the GST purification was dialyzed against buffer for HRV 3C protease (50 mM Tris-HCl pH 7.0, 150 mM NaCl, 1 mM EDTA, 1 mM DTT), and the GST tag was removed

Author Manuscript Author Manuscript Author Manuscript Author Manuscript

by HRV 3C protease (GE Healthcare, Chicago IL, USA). After the protease cleavage, the protein was purified with Ni Sepharose® (GE Healthcare, Chicago IL, USA) in accord with the supplier recommended procedure. The purified protein was dialyzed against buffer for HDX/MS (8.3 mM Tris pH7.2, 50 mM NaCl 10% glycerol) and was concentrated by Amicon® Ultra (Milliporesigma, Burlington MA, USA) up to 1.5 mg/ml.

Hydrogen-deuterium exchange mass spectrometry

The experiments were performed by following the methods previously published [34]. In brief, 2 μl of protein solution was incubated with 1 μl of 13 mM EGCG or αToc in the buffer for HDX/MS for 20 min at 25°C. The following steps were performed at 4°C. The deuterium exchange was initiated by adding 9 μl of D_2O buffer (8.3 mM Tris-HCl pD 7.2, 50 mM NaCl, in 98% D_2O). The exchange solution was quenched after 10, 100, 1000, and 10000 seconds with 18 μl of quenching solution (0.08 M guanidine HCl, 0.8% formic acid, 16.6% glycerol), and the sample was immediately frozen using dry ice. The sample was kept at −80°C until subjecting to proteolysis liquid chromatography-mass spectrometry analysis using the pepsin column. The data were analyzed using Proteom Discoverer software (Thermo Fisher LLC, San Jose CA, USA) and DXMS Explorer (Sierra Analytics Inc., Salida CA, USA) by following the previous report [34]. HDX/MS experiment was performed twice using independent batches of purified 67LR protein, and reproducible peptide regions are shown.

Receptor-membrane systems

The Membrane Builder implemented in CHARMM-GUI was employed to generate 3D models for the MD simulations [35,36]. The membrane patch consisted of phosphocholine (PC), phosphoethanolamine (PE), phosphoserine (PS), phosphoinositol (PI), and sphingomyelin (SPH). The membrane composition was selected based on the localization of 67LR on cellular membranes according to previously published data [37,38]. Each system was solvated with TIP3P water molecules and neutralized with 150 mM sodium chloride (NaCl) using the Visual Molecular Dynamics (VMD) package [39].

Equilibration and production run.

Molecular dynamics simulations were carried out using NAMD 2.12 [40]. The following minimization and equilibration protocol was performed: a minimization of 80,000 steps was initially performed by applying harmonic constraints on the receptor-ligand-membrane that were gradually turned off using a constraint scaling factor, followed by a second 120,000 steps minimization without constraints. An initial equilibration of 10,000 steps was performed by also applying harmonic constraints on the receptor-ligand-membrane that were gradually turned off using the same constraint scaling factor, followed by a second 10,000 steps equilibration without constraints. During the equilibration, each system was slowly heated and held to 310 K using a temperature reassignment with a reassignment frequency of 500-time steps (1000 fs) and a reassignment increment of 1 K. The above minimization and equilibration protocol was sufficient to induce the appropriate disorder of a fluid-like bilayer, avoid unnatural atomistic positions, and failure of the simulations by atoms moving at very high velocities. Each system was finally subjected to a 1 μs production run. For each production run, the temperature was maintained at 310 K using the Langevin thermostat

Author Manuscript Author Manuscript Author Manuscript Author Manuscript

with the Langevin coupling coefficient of 1/ps [41]. The NPT ensemble was employed, and the pressure was kept constant at 1.01325 kPa using the Langevin piston method with the “useGroupPressure,” “useFlexibleCell,” and “useConstantArea” parameters turned on [42]. A time step of 2 fs was used in combination with the SHAKE algorithm to hold the bonds of hydrogen atoms similarly constrained [43]. Nonbonded interactions and full electrostatics were calculated every 1 and 2-time steps, respectively. Switching functions are used to smoothly take electrostatic and van der Waals interactions to zero with a switching distance of 10 Å and a cutoff of 12 Å. Long-range electrostatic forces in the periodic system were evaluated using the Particle Mesh Ewald (PME) Sum method with grid spacing 1/Å [44]. The CHARMM General Force Field (CGenFF) and the CHARMM36 all-atom additive force field and parameters were used for the simulations [45,46]. The simulation was run twice with the same settings. The main figures are generated from the first simulation.

Cell viability assay

HCT116 cells were inoculated in 60 mm dishes with 2.0×10^5 cell/dish and cultured for 48 h. The medium was changed so as to include various concentrations of EGCG or αToc in a fresh medium. After 48 h incubation, the number of viable cells was counted. When the endogenous 67LR was knocked down, siRNA targeting 67LR was transfected 24 h after inoculating the cells using the same method described above.

Statistical analysis

All error bars show standard error of the mean (SEM). Student’s t-test was carried out when comparing two data sets. One-way ANOVA followed by Dunnet’s multiple comparison test was carried out when the experiment had more than three groups using BellCurve for Excel Version 3.20. A *p*-value of less than 0.05 was considered to be significant.

RESULTS

DGKα activation by αToc through 67LR

Vitamin E consists of four tocopherols and four tocotrienols classified α, β, γ, and δ by the position of the methyl moieties on the chroman ring structure. αToc is a hydrophobic compound that has three methyl moieties on positions 5, 7, and 8 of the chroman ring (Fig. 1a). αToc induces translocation of GFP-tagged DGKα to the plasma membrane, which is a hallmark of DGKα activation (Fig. 1b) [10]. To investigate if 67LR contributes to the translocation, cells were pretreated with 67LR antibody which blocks GFP-DGKα translocation by EGCG [24], and αToc-induced translocation of GFP-DGKα was monitored. The pretreatment of the 67LR antibody significantly inhibited the translocation induced by αToc (Fig. 1c), suggesting αToc activates DGKα via 67LR. Indeed, the knockdown of endogenous 67LR by siRNA also significantly attenuated the translocation of DGKα (Fig. 1d). Also, we tested the effect of all tocopherols on the translocation of DGKα, and revealed that not only αToc but also the other tocopherols induced translocation of GFP-DGKα to the plasma membrane (Fig. 1e). Then, we compared the translocation efficiency induced by all tocopherols and found that they had a similar effect on the DGKα translocation (Fig. 1f). These results indicated that all tocopherols

Author Manuscript Author Manuscript Author Manuscript Author Manuscript

induce DGKα activation via 67LR and the possibility that 67LR acts as a receptor for tocopherols.

Direct binding of αToc to 67LR and its affinity

We investigated the direct binding of αToc to 67LR and its affinity by various approaches. It has been reported that 67LR is a matured dimer form of the 37 kDa laminin receptor precursor (37LRP), but the detailed relationship was not understood [47]. Note that, in the present study, we employed cDNA encoded 37LRP to express recombinant 67LR. First, we precipitated FLAG-tagged recombinant 67LR by FLAG tag antibody-conjugated beads, and the beads were incubated with αToc. The ratio of bound αToc to precipitated 67LR was analyzed by HPLC. FLAG-tagged α-TTP was used as a positive control. Consequently, a significant amount of αToc was detected in both FLAG-67LR and FLAG-α-TTP precipitated beads comparing to FLAG tag alone (Fig. 2a). In addition, the amount of bound αToc increased concentration-dependently (Fig. 2b). Next, we made tocopherol conjugated beads and analyzed the amount of FLAG-67LR bound to the tocopherol beads. The scheme for the production of tocopherol conjugated beads is shown in Fig. S3. Control beads and tocopherol conjugated beads were incubated with lysate of FLAG-67LR overexpressed cells, and the bound FLAG-67LR was detected by western blot. Although some amount of FLAG-67LR nonspecifically bound to the control beads, significantly more FLAG-67LR was detected with the tocopherol conjugated beads (Fig. 2c). While, α-TTP did not bind to the tocopherol conjugated beads (data not shown). This might be related to the binding mode of αToc in α-TTP [48,49].

Further, to confirm the binding, we performed a differential scanning fluorometry (DSF) using 10 μM purified recombinant GST-67LR-His protein. Two independent peaks showing the Tm value of protein, which might be delivered from 67LR and GST tag protein, were detected (Fig. S5). The first peak shifted to 1 °C and 2 °C higher temperature in the presence of 10 μM and 100 μM αToc, respectively, and αToc did not show any effect on the second peak (Fig. S5a). Importantly, although 10 μM EGCG did not show any effect, 100 μM EGCG increased the Tm value of the first peak without any effect on the second peak (Fig. S5b). These results indicated that the first peak shows the Tm value of 67LR, and EGCG and αToc increase the thermal stability of 67LR by direct binding. Finally, to measure the affinity of αToc to 67LR, we carried out the isothermal titration calorimetry (ITC). By titrating the 120 μM purified GST-67LR-His to 20 μM αToc in the sample cell, absorption of heat by the interaction of αToc to 67LR was detected, and the absorption disappeared eventually due to the saturation of the ligand (Fig. 2d). The sigmoid curve was obtained by processing the area under the curve of each peak, and the mean of K_d value was 788 ± 174 nM (Fig. 2e). Notably, the heat of dilution from αToc and GST-67LR-His was not significant (Fig S6a, b). These approaches successfully demonstrated the direct binding of αToc to 67LR and its affinity.

αToc binding site of 67LR

Having shown that αToc directly binds to 67LR, we then investigated exactly how αToc binds to 67LR. The putative EGCG binding motif of 67LR and the mutations which abolish binding to EGCG, such as the Lys166Glu mutant, have been reported, although

Author Manuscript Author Manuscript Author Manuscript Author Manuscript

the detailed binding model of EGCG was not known [50]. To address this question, we constructed a FLAG-67LR Lys166Glu mutant and observed its effect on the translocation of DGKα induced by EGCG and αToc. We checked if FLAG-tagged 67LR localizes at the plasma membrane and observed membrane localization of FLAG-67LR at the plasma membrane (Fig. S7). When the mutant was overexpressed, the rate of the EGCG-induced DGKα translocation was significantly less than with wild-type overexpressing cells (Fig. 3a), confirming that Lys166 is critical for the binding to EGCG. In contrast, αToc-induced translocation with overexpression of the mutant was the same as that with overexpression of the wild type (Fig. 3b). These results suggested that the αToc binding site of 67LR is different from that of EGCG. Then, we performed a docking simulation of the EGCG and αToc to the putative EGCG binding site employing Glide software and the crystal structure of 67LR [51]. The putative EGCG binding site is in a water-exposed hydrophilic region, and EGCG docks to the binding site with several hydrogen bonds (Fig. 3c, d). Indeed, the XP GScore, which represents binding stability, was decent (−6.723). However, αToc did not dock well to the binding site based on a poor XP GScore (−0.623) (Fig. 3e), suggesting that the αToc binding site in the 67LR is different from that of EGCG.

We then carried out HDX/MS experiments to locate the αToc binding site on 67LR experimentally. Also, we aimed to confirm the EGCG binding site on 67LR by HDX/MS. The effect of the presence of αToc or EGCG on the deuterium exchange ratio was analyzed by comparing the deuterium level in the absence of ligands. The peptide regions which included Lys11 to Lys17, Asn50 to Ala61, and Trp176 to Leu183 in the α-helices were inhibited after deuterium exchange by the presence of αToc while, significant decreases in the number of deuterium were not observed in the neighboring peptides to these regions such as Phe16 to Thr28, Phe32 to Ile46, and Leu183 to Tyr202 (Fig. 3f). These residues appeared to form a reasonable pocket for αToc, suggesting this region as a probable αToc binding site. In the case of EGCG, significant inhibition of deuterium exchange in the regions including residues Leu16 to Met34 and Ile161 to Gly172 that are close to the putative EGCG binding site was confirmed compared to the neighboring peptides such as Gly-5 (linker region) to Gln9 and Leu183 to Leu203 that showed no inhibition (Fig. 3g).

Binding mode of αToc and EGCG in 67LR

MD simulations were carried out to elucidate if and how αToc docks to the region suggested by HDX/MS. We created a model of 67LR in a lipid bilayer using CHARMM-GUI Membrane Builder, with the composition of the lipid bilayer mimicking that of lipid rafts based since 67LR is present in lipid rafts [38]. In the model, 67LR penetrated the lipid bilayer, but the predicted EGCG binding site was exposed to water (Fig. S8 and S9b). Based on the model and the results of HDX/MS, the initial position of αToc was placed in the lipid bilayer near the region we experimentally determined (Fig. S9a), and the initial position of EGCG was placed exposed to the water near the putative binding site since EGCG is a water-soluble compound (Fig. S9b).

In the simulation of αToc, αToc drifted in the lipid bilayer at the beginning of the simulation but gradually approached the putative binding region (Movie S1). Finally, αToc bound to 67LR by penetrating its phytyl moiety into the α-helix assembling region (Movie S1). The

Author Manuscript Author Manuscript Author Manuscript Author Manuscript

optimal binding mode showed that the phytyl moiety of αToc completely penetrated the putative binding region of 67LR (Fig. 4a). When αToc approached the binding site, the chroman ring structure faced to Phe203, and the phytyl moiety then got inside afterward (Movie S2). Finally, the aromatic residues such as Trp176, Phe203, and Tyr202 packed the chroman ring and would stabilize the binding (Fig. 4b). The 2D binding analysis of its optimal binding mode revealed that the backbone of Tyr202 interacts with the hydroxy group of the chroman ring structure with relatively weak hydrogen bonds (donor-acceptor distance: 2.99Å, donor-hydrogen-acceptor angle: 151.2°), and a hydrophobic pocket formed containing Phe18, Trp55, Lys17, Leu58, Trp176, and Met177 accommodate the phytyl moiety (Fig. S10a). We repeated the simulation to confirm the result, and the second simulation was well consistent with the first simulation. In brief, the phytyl moiety of αToc got into the hydrophobic pocket with similar movement (Movie. S3). In the second run, π-H interactions were detected on Trp176 and Phe18, while hydrogen bonds between Phe202 was not detected (Fig. S10c). Importantly, the same hydrophobic pocket accommodated αToc in both simulations.

In the EGCG binding simulation, EGCG approached its binding site and bound to the putative EGCG binding region which includes the region found by HDX/MS (Movie S4 and Fig. 4c). The simulation also confirmed an interaction between the galloyl moiety of EGCG and Lys166 in the optimal binding mode (Fig. 4d and Movie S5). In addition, it was turned out that Asp126 and Asp151 frequently interacted with the B-ring and galloyl moiety of EGCG, respectively, by hydrogen bonds (Fig. 4d and Movie S5). In the optimal binding mode, the galloyl moiety formed strong hydrogen bonds with Asp151 (donor-acceptor distance: 2.47Å, donor-hydrogen-acceptor angle: 164.3°). In addition to these residues, Asn149 and Asn165 were also contributing to the binding of EGCG by interacting with the galloyl moiety (Fig. S10b). The second simulation also showed a similar binding mode with the first run (Movie S6). Notably, although there are some differences in the hydrogen bond pair, Asp126, Asp151, Asn165, and Lys166 formed hydrogen bonds with B ring or galloyl moiety, indicating that these residues are critical for EGCG binding (Fig. 10d).

The effect of mutations in the αToc binding pocket of 67LR on DGKα translocation

To confirm the identity of the αToc binding site of 67LR, we constructed several point mutants of 67LR based on the optimal binding mode from MD simulation (Fig. 5a) and observed the effect of overexpression of the mutants on the αToc and EGCG-induced translocation of GFP-DGKα. Consistent with the results in Fig. 3a and b, overexpression of Lys166Glu, as well as wild-type (WT) 67LR showed significantly enhanced αToc-induced translocation of DGKα comparing to the control, while overexpression of Lys166Glu showed no effect on EGCG-induced translocation (Fig. 5b, c), indicating Lys166, contributes EGCG binding but not αToc binding as HDX/MS and MD simulation revealed. First, among the regions suggested by HDX/MS and MD simulations for αToc binding, we tested the mutants of Trp55 and Trp176. The former is in the hydrophobic pocket, and the latter is close to the chroman ring structure (Fig. 4b and Fig. 5a). These mutants did not enhance the αToc-induced translocation of DGKα (Fig. 5b), indicating that these residues contribute to the binding of αToc. In addition, we tested two mutants that are close to the region accommodating the chroman ring structure but seemed not to be essential

Author Manuscript Author Manuscript Author Manuscript Author Manuscript

for the binding, such as Phe90 and Lys89, to confirm the accuracy of the binding model from the MD simulations (Fig. 5a). Although there is no statistical significance, Phe90Ala showed a tendency to enhance αToc-induced translocation, while Lys89Ala significantly enhanced the translocation (Fig. 5b). These results suggest that Phe90 partly contributes to the binding of αToc, but it is not essential and that Lys89 does not contribute to the binding of αToc as MD simulation indicated. Indeed, the distance from the chroman ring to Lys89 is much longer (more than 6 Å) than that to Phe90 (5.63 Å) in the optimal binding mode of αToc. Notably, these mutants, except for Lys166Glu, significantly enhanced the EGCG-induced translocation of DGKα as WT, confirming that the mutants only affected the binding to αToc (Fig. 5c). From these results, it is clear that Trp55, Phe90, and Trp176 are in the putative αToc binding site suggested by HDX/MS and MD simulations and are partly or critically contributing to the αToc binding, confirming that the proposed binding mode of αToc in 67LR is reasonable.

The involvement of 67LR in the anticancer effect of tocopherols

To seek another physiological role of αToc-67LR binding, we focused on the anticancer effect of tocopherols. It has been reported that tocopherols, especially γToc, δToc, and tocopherol derivatives, exhibit the anticancer effect [52–56]. However, the mechanisms are not completely understood. On the one hand, it is well known that EGCG exhibits anticancer effects, and 67LR is a target of the effect [21,22]. Since all tocopherols and derivatives induce the DGKα translocation, these compounds can bind to 67LR. Therefore, we ask if the anticancer effect of tocopherols is mediated through 67LR. It is known that the expression of 67LR is upregulated with the progression of human colon cancer [23]. We treated HCT116 human colon cancer cells with various concentrations of EGCG and αToc and measured cell viability. EGCG significantly suppressed the cell viability at 50 μM (Fig. 6a), and αToc showed a significant effect on the viability at greater than 100 μM, although the effect was weak (Fig. 6b). Then, we tested the effect of 50 μM EGCG and 100 μM αToc on the viability of HCT116 cells with or without siRNA knockdown of 67LR. EGCG and αToc were treated 24 h after siRNA transfection for 48 h. We confirmed that the expression level of 67LR was downregulated by 48h after siRNA-transfection, although the expression was recovered by 72h (Fig. 6c). The effect of EGCG on HCT116 cells was eliminated by the knockdown of 67LR (Fig. 6d). Similarly, the effect of αToc on HCT116 was also eliminated by the 67LR knockdown (Fig. 6e). These results revealed that 67LR is involved at least in the observed cell growth inhibition effects of 100 μM αToc in addition to the DGKα activation effect. However, the role of 67LR in the anticancer effects of αToc as well as other tocopherol species requires further investigation.

DISCUSSION

It has been of longstanding scientific interest to understand exactly how vitamin E and, in particular, αToc expresses its non-antioxidant functions, such as activation of specific signal transduction. Several studies have shown that αToc interacts with plasma membranes and expresses its function by affecting membrane formation and stability [57,58]. However, the mechanism of just how αToc is involved in various signal transduction processes, especially at a structural level, was not understood. In this study, we have demonstrated that αToc

Author Manuscript Author Manuscript Author Manuscript Author Manuscript

directly binds to 67LR, and we have identified a putative αToc binding site on 67LR. HDX/MS and MD simulations were used to reveal the binding mode of αToc. In addition, we have discovered that 67LR functions as an αToc receptor as well as an EGCG receptor. These results clearly indicate for the first time that 67LR is one of the pathways involved in the function of αToc and other tocopherols. Moreover, we have demonstrated in detail the binding mode of EGCG to its previously proposed binding site on 67LR by employing HDX/MS and MD simulations.

Several downstream signaling pathways of 67LR have been reported [21,59]. However, it is still unclear how 67LR activates its downstream pathways. Our previous study revealed that the Src family tyrosine kinase is involved in the αToc-induced DGKα activation [10]. Recently, we have reported that Src family tyrosine kinase interacts with 67LR and mediates the EGCG-induced DGKα activation as with αToc [25]. Further, Kumazoe *et al.* also reported the implementation of Src in the signaling pathway of 67LR [25]. Therefore, the Src family tyrosine kinase should be one of the downstream pathways of αToc-67LR interaction. However, the binding sites of 67LR for EGCG and αToc are different from one another. Therefore, it is still an open question how two different binding sites trigger the same signaling pathway.

It has been recognized that αToc initiates signal transduction by inhibiting PKC in cells, and the effect was not attributed to its antioxidant effect. However, the detailed mechanisms were enigmatic [5,60]. We have demonstrated herein that αToc-67LR interaction activates DGKα, which can effectively inhibit PKC activity by converting diacylglycerol (DAG), an activator of PKC into phosphatidic acid (PA) [61]. Therefore, activation of the αToc-67LR-DGKα pathway can indirectly lead to PKC inhibition, thereby resulting in a downstream physiological role for αToc.

By employing the ITC approach, we demonstrated the K_d value of αToc to 67LR as 788 ± 174 nM. The K_d value of EGCG has been shown by the surface plasmon resonance (SPR) as 39.9 nM [18]. The affinity of αToc seemed to be relatively lower than that of EGCG. However, since αToc is a vitamin, the basal concentration of αToc in the human plasma is kept at 10 to 30 μM [62]. In contrast, the maximum plasma concentration of EGCG does not exceed 1 μM even after several cups of tea consumption [63]. Regarding the difference in the plasma concentration, the gap in the affinity of these two ligands to 67LR seemed to be reasonable. The affinity of αToc to α-TTP has been reported as 36.1 nM [64]. As described above, α-TTP plays a central role in the absorption of αToc, and the deficiency or impaired function of α-TTP cause AVED [6–8]. Therefore, it is proper that α-TTP possesses a higher affinity for αToc than that of 67LR, which is one of the pathways expressing the function of αToc. Also, it is well known that αToc is mainly associating with lipoproteins in human plasma and transported into the cell through lipoprotein receptors [65]. Therefore, how monomeric αToc accesses the cell membrane where 67LR is expressed requires future investigation.

To evaluate the translocation of GFP-DGKα in this study, we used a higher concentration of αToc to observe a clear translocation. Note that GFP-DGKα translocation was observed at a physiological concentration (10 μM) of αToc (data not shown). Indeed, we reported

Author Manuscript Author Manuscript Author Manuscript Author Manuscript

that αToc ameliorates diabetic nephropathy through DGKα *in vivo* using DGKα knockout mice [11], and that oral consumption of αToc ameliorated diabetic nephropathy in mice [66]. Also, the inhibition of diabetes-induced PKC activation is observed in mice with the oral administration of αToc [66]. Therefore, a physiological concentration of αToc should activate DGKα through 67LR *in vivo*.

It has been reported that the anticancer effect of αToc is weak or not observed *in vivo* [53,54,67,68]. Indeed, in this study, less than 100 μM αToc which is above the physiological concentration, did not significantly affect the HCT116 cell viability. On the one hand, it has been reported that γToc and δToc not αToc showed an anticancer effect *in vivo* and suggested that the ability to trap reactive oxygen and nitrogen species of them make a difference in the effect [54]. Since all tocopherols showed a similar effect on the DGKα translocation (Fig. 1f), they might have a similar affinity to 67LR. Accordingly, although there is some contribution, the contribution of 67LR to the anticancer effect of tocopherols seemed not to be dominant. For the physiological role of αToc-67LR binding other than DGKα activation will be needed further investigations.

This study successfully employed HDX/MS to experimentally determine how EGCG and αToc bind to separate and distinct binding sites on 67LR, one hydrophobic and one hydrophilic. In the HDX/MS experiments, the degree of inhibition of deuterium exchange by αToc was less than was observed by EGCG (Fig. 3f, g), though this was on different peptides at different sites. Since the source of deuterium is D_2O in the HDX/MS experiments, water accessibility contributes to the rate and amount of deuterium exchange. Therefore, more water-accessible regions can be more sensitive to the inhibition in the deuterium exchange in the presence of ligands or morphological changes. Indeed, the EGCG binding region is highly water accessible whereas, the αToc binding region exists in a hydrophobic part of 67LR, which is closed until αToc accesses the binding site. These differences in physical characteristics might contribute to the difference in the degree of inhibition during deuterium exchange.

It has been reported that 67LR is formed by homodimers of 37LRP, and dimerization is important for membrane localization [16,47,51,69]. However, the actual formation of a dimer and the membrane binding conformation are not entirely understood. We attempted to use the putative formation of a 67LR homodimer suggested by the crystal structure for the MD simulations. However, the dimer structure did not properly fit in the lipid bilayer *in silico*. Therefore, we had to take advantage of the monomer structure of 67LR (37LRP). However, we successfully observed direct binding between monomer 67LR and αToc and the binding mode between monomer 67LR and EGCG and αToc in the MD simulations. These facts suggest that dimer formation is important for activating 67LR downstream or localization at the membrane, but not for binding to αToc and EGCG.

At the beginning of the binding of αToc to 67LR, the chroman ring structure faced to Phe203 and Trp176 which are at the entrance of the αToc binding site, and this step appeared to be critical to guide αToc to the hydrophobic site. Indeed, overexpressing the Trp176Ala mutant failed to increase the αToc-induced translocation of DGKα (Fig. 5b), and the importance of the chroman ring structure was consistent with a previous report

Author Manuscript Author Manuscript Author Manuscript Author Manuscript

[10]. Thereafter, the phytyl moiety entered into the binding site. In other words, both the chroman ring structure and the phytyl moiety are essential for αToc binding to 67LR, and the position of the methyl moiety on the chroman ring structure seems to not contribute to the binding. Indeed, docking simulation using the other tocopherols revealed that the binding poses and binding scores of all tocopherols are similar to each other (Fig. S11). In other words, all tocopherols could bind to 67LR with a similar affinity regardless of the position and number of the methyl groups on the chroman ring. This result was consistent with the result that the other tocopherols induced translocation of DGKα as well as αToc (Fig. 1e, f) and suggesting that 67LR could well be the receptor for all tocopherols.

Amino acid residues 161 to 180 are well known as a laminin-binding domain named "peptide G," and the reported EGCG binding motif was contained within peptide G [50,70]. The binding mode revealed that Lys166 and Asn165 in the previously predicted EGCG binding motif and Asp151 that was not known as a binding residue, are critical for binding with galloyl moiety of EGCG. It is well known that 67LR binds only to catechins with a galloyl moiety [18], and these residues may contribute to the selectivity of 67LR for catechins. In addition to these interactions, the MD simulation showed that the hydroxy group on the B ring of EGCG firmly and frequently interacted with Asp126 which has not been reported as a binding region. Also, Asp151 formed a hydrogen bond with the B ring in the second simulation (Fig. S10d). It is reported that EGCG has the best affinity to 67LR among catechins, and catechins which have three hydroxy groups on the B ring have a higher affinity than catechins which have two hydroxy groups on the B ring [71]. Thus, the variation in the affinity may occur because of the differences in the number of hydroxy groups on the B ring, which can interact with these residues. Indeed, all three hydroxy groups on the B ring were occupied with hydrogen bonds with Asp126 and Asp151 in the binding mode from the second simulation (Fig S10d). In other words, Asp126 and Asp151 contribute to the strength of the 67LR affinity to the catechins based on the number of hydroxy groups on the B ring.

As described above, it is well recognized that EGCG functions as an anticancer agent through 67LR, and EGCG-67LR binding is expected as an attractive target for treating various cancer [19–23]. However, the low stability and absorption of EGCG in the human plasma has been a critical issue for the usage of EGCG as an anticancer agent. In the present study, we showed the detailed binding mode of EGCG for the first time, and the binding mode was reasonable and consistent with previous reports. Therefore, now it should be possible to produce optimal agonists of 67LR based on our binding model using structure-based drug design approaches.

CONCLUSION

This study clearly shows for the first time that αToc directly binds to the hydrophobic binding site of 67LR, which is different from the hydrophilic binding site for EGCG, and that 67LR mediates DGKα activation (Fig. 7). Also, it is suggested that 67LR contributes to the anticancer effect of αToc at least in vitro at a high concentration of αToc (Fig. 7). This explains one of the pathways for how αToc expresses non-oxidative functions through the

Author Manuscript Author Manuscript Author Manuscript Author Manuscript

cell surface receptor, and provides important insights that should help establish the complete picture of the functioning of vitamin E in metabolism.

Supplementary Material

Refer to Web version on PubMed Central for supplementary material.

ACKNOWLEDGEMENT

We gratefully acknowledge Dr. Brenda Andrade and Prof. Michael K. Gilson at University of California San Diego, Skaggs School of Pharmacy and Pharmaceutical Sciences, and Dr. Simon Bergqvist at Biofizik, Inc. for helping with the affinity measurement experiments. We sincerely thank Dr. Daizo Hamada at Kobe University for helping with the purification of 67LR, and Taiyo Kagaku Co. Ltd. (Japan) and Eisai Co. Ltd. (Japan) for providing information on EGCG and vitamin E.

Funding source:

This work was supported by a Grant-in-Aid from the Japan Society for the Promotion of Science (JSPS) Fellow Grant Number JP16J02115 (D.H.) and partly supported by the Honjo International Scholarship Foundation (Y.S.). The HDX/MS and MD simulations were supported by NIH grant GM20501–45 and R35 GM139641–02 (E.A.D.).

REFERENCES

[1]. Rigotti A Absorption, transport, and tissue delivery of vitamin E. Mol Aspects Med 2007. 10.1016/j.mam.2007.01.002.

[2]. Traber MG, Atkinson J. Vitamin E, antioxidant and nothing more. Free Radic Biol Med 2007;43:4–15. 10.1016/j.freeradbiomed.2007.03.024. [PubMed: 17561088]

[3]. Azzi A, Stocker A. Vitamin E : non-antioxidant roles 2000;39:231–55.

[4]. Landes N, Pfluger P, Kluth D, Birringer M, Rühl R, Böl GF, et al. Vitamin E activates gene expression via the pregnane X receptor. Biochem Pharmacol 2003;65:269–73. 10.1016/S0006-2952(02)01520-4. [PubMed: 12504802]

[5]. Tasinato A, Boscoboinik D, Bartoli GM, Maroni P, Azzi A. d-α-tocopherol inhibition of vascular smooth muscle cell proliferation occurs at physiological concentrations, correlates with protein kinase C inhibition, and is independent of its antioxidant properties. Proc Natl Acad Sci U S A 1995;92:12190–4. 10.1073/pnas.92.26.12190. [PubMed: 8618868]

[6]. Sato Y, Hagiwara K, Arai H, Inoue K. Purification and characterization of the α-tocopherol transfer protein from rat liver. FEBS Lett 1991;288:41–5. 10.1016/0014-5793(91)80999-J. [PubMed: 1879562]

[7]. Hosomi A, Arita M, Sato Y, Kiyose C, Ueda T, Igarashi O, et al. Affinity for α-tocopherol transfer protein as a determinant of the biological activities of vitamin E analogs. FEBS Lett 1997;409:105–8. 10.1016/S0014-5793(97)00499-7. [PubMed: 9199513]

[8]. Ouahchi K, Arita M, Kayden H, Ben Hamida M, Sokop R, Araf H, et al. Ataxia with isolated vitamin E deficiency is caused by mutations in the a-tocopherol transfer protein. Nat Genet 1995;9:141–5. [PubMed: 7719340]

[9]. Koya D, Lee IK, Ishii H, Kanoh H, King GL. Prevention of glomerular dysfunction in diabetic rats by treatment with d-alpha-tocopherol. J Am Soc Nephrol 1997;8:426–35. [PubMed: 9071711]

[10]. Fukunaga-Takenaka R, Shirai Y, Yagi K, Adachi N, Sakai N, Merino E, et al. Importance of chroman ring and tyrosine phosphorylation in the subtype-specific translocation and activation of diacylglycerol kinase α by D-α-tocopherol. Genes to Cells 2005;10:311–9. 10.1111/j.1365-2443.2005.00842.x. [PubMed: 15773894]

[11]. Hayashi D, Yagi K, Song C, Ueda S, Yamanoue M, Topham M, et al. Diacylglycerol Kinase alpha is Involved in the Vitamin E-Induced Amelioration of Diabetic Nephropathy in Mice. Sci Rep 2017;7:2597. 10.1038/s41598-017-02354-3. [PubMed: 28572624]

[12]. Kakehi T, Yagi K, Saito N, Shirai Y. Effects of vitamin E and its derivatives on diabetic nephropathy in Rats and identification of diacylglycerol kinase subtype involved

Author Manuscript Author Manuscript Author Manuscript Author Manuscript

in the improvement of diabetic nephropathy. Funct Foods Heal Dis 2018;7:816. 10.31989/ffhd.v7i10.386.

[13]. Rao NC, Barsky SH, Terranova VP, Liotta LA. Isolation of a tumor cell laminin receptor. Biochem Biophys Res Commun 1983;111:804–8. 10.1016/0006-291X(83)91370-0. [PubMed: 6301485]

[14]. Malinoff HL, Wicha MS. Isolation of a cell surface receptor protein for laminin from murine fibrosarcoma cells. J Cell Biol 1983;96:1475–9. 10.1083/jcb.96.5.1475. [PubMed: 6302102]

[15]. Lesot H, Kühl U, von der Mark K, Mark K. Isolation of a laminin-binding protein from muscle cell membranes. EMBO J 2018;2:861–5. 10.1002/j.1460-2075.1983.tb01514.x.

[16]. Gauczynski S, Peyrin J, Haõ Â, Leucht C, Hundt C, Rieger R, et al. The 37-kDa / 67-kDa laminin receptor acts as the cell-surface receptor for the cellular prion protein. EMBO J 2001;20:5863–75. [PubMed: 11689427]

[17]. Wang KS, Kuhn RJ, Strauss EG, Ou S, Strauss JH. High-affinity laminin receptor is a receptor for Sindbis virus in mammalian cells. J Virol 1992;66:4992–5001. [PubMed: 1385835]

[18]. Tachibana H, Koga K, Fujimura Y, Yamada K. A receptor for green tea polyphenol EGCG. Nat Struct Mol Biol 2004;11:380–1. 10.1038/nsmb743. [PubMed: 15024383]

[19]. Hand PH, Thor A, Schlom J, Rao CN, Liotta L. Expression of Laminin Receptor in Normal and Carcinomatous Human Tissues as Defined by a Monoclonal Antibody. Cancer Res 1985;45:2713–9. [PubMed: 3157447]

[20]. Cioce V, Castronovo V, Shmookler BM, Garbisa S, Grigioni WF, Liotta L a, et al. Increased expression of the laminin receptor in human colon cancer. J Natl Cancer Inst 1991;83:29–36. [PubMed: 1824600]

[21]. Umeda D, Yano S, Yamada K, Tachibana H. Green tea polyphenol epigallocatechin-3-gallate signaling pathway through 67-kDa laminin receptor. J Biol Chem 2008;283:3050–8. 10.1074/jbc.M707892200. [PubMed: 18079119]

[22]. Kumazoe M, Sugihara K, Tsukamoto S, Huang Y, Tsurudome Y, Suzuki T, et al. 67-kDa laminin receptor increases cGMP to induce cancer-selective apoptosis. J Clin Invest 2013;123:787–99. 10.1172/JCI64768. [PubMed: 23348740]

[23]. Sanjuán X, Fernández PL, Miquel R, Muñoz J, Castronovo V, Ménard S, et al. Overexpression of the 67-kD laminin receptor correlates with tumour progression in human colorectal carcinoma. J Pathol 1996;179:376–80. 10.1002/(SICI)1096-9896(199608)179:4<376::AID-PATH591>3.0.CO;2-V. [PubMed: 8869283]

[24]. Hayashi D, Ueda S, Yamanoue M, Saito N, Ashida H, Shirai Y. Epigallocatechin-3-gallate activates diacylglycerol kinase alpha via a 67 kDa laminin receptor: A possibility of galloylated catechins as functional food to prevent and/or improve diabetic renal dysfunctions. J Funct Foods 2015;15. 10.1016/j.jff.2015.04.005.

[25]. Hayashi D, Wang L, Ueda S, Yamanoue M, Ashida H. The mechanisms of ameliorating effect of a green tea polyphenol on diabetic nephropathy based on diacylglycerol kinase α. Sci Rep 2020;10:11790. 10.1038/s41598-020-68716-6. [PubMed: 32678222]

[26]. Masson GR, Burke JE, Ahn NG, Anand GS, Borchers C, Brier S, et al. Recommendations for performing, interpreting and reporting hydrogen deuterium exchange mass spectrometry (HDX-MS) experiments. Nat Methods 2019;16:595–602. 10.1038/s41592-019-0459-y. [PubMed: 31249422]

[27]. Wang L, Smith DL. Probing Protein Structure and Dynamics by Hydrogen Exchange-Mass Spectrometry. Curr. Protoc. Protein Sci, 2002, p. 17.6.1–17.6.18. 10.1002/0471140864.ps1706s28.

[28]. Chambers E, McFerran NV, Steele D, Doherty C, Nelson J, Timson DJ, et al. The 67 kDa laminin receptor: structure, function and role in disease. Biosci Rep 2008;28:33. 10.1042/bsr20070004. [PubMed: 18269348]

[29]. Mouchlis VD, Chen Y, Andrew McCammon J, Dennis EA. Membrane Allostery and Unique Hydrophobic Sites Promote Enzyme Substrate Specificity. J Am Chem Soc 2018;140:3285–91. 10.1021/jacs.7b12045. [PubMed: 29342349]

Author Manuscript Author Manuscript Author Manuscript Author Manuscript

[30]. Madhavi Sastry G, Adzhigirey M, Day T, Annabhimoju R, Sherman W. Protein and ligand preparation: Parameters, protocols, and influence on virtual screening enrichments. J Comput Aided Mol Des 2013;27:221–34. 10.1007/s10822-013-9644-8. [PubMed: 23579614]

[31]. Mouchlis VD, Limnios D, Kokotou MG, Barbayianni E, Kokotos G, McCammon JA, et al. Development of Potent and Selective Inhibitors for Group VIA Calcium-Independent Phospholipase A2 Guided by Molecular Dynamics and Structure-Activity Relationships. J Med Chem 2016;59:4403–14. 10.1021/acs.jmedchem.6b00377. [PubMed: 27087127]

[32]. Mouchlis VD, Morisseau C, Hammock BD, Li S, McCammon JA, Dennis EA. Computer-aided drug design guided by hydrogen/deuterium exchange mass spectrometry: A powerful combination for the development of potent and selective inhibitors of Group VIA calcium-independent phospholipase A2. Bioorganic Med Chem 2016;24:4801–11. 10.1016/j.bmc.2016.05.009.

[33]. Halgren TA, Murphy RB, Friesner RA, Beard HS, Frye LL, Pollard WT, et al. Glide: A New Approach for Rapid, Accurate Docking and Scoring. 2. Enrichment Factors in Database Screening. J Med Chem 2004;47:1750–9. 10.1021/jm030644s. [PubMed: 15027866]

[34]. Burke JE, Hsu YH, Deems RA, Li S, Woods VL, Dennis EA. A phospholipid substrate molecule residing in the membrane surface mediates opening of the lid region in group IVA cytosolic phospholipase A2. J Biol Chem 2008;283:31227–36. 10.1074/jbc.M804492200. [PubMed: 18753135]

[35]. Wu EL, Cheng X, Jo S, Rui H, Song KC, Dávila-Contreras EM, et al. CHARMM-GUI membrane builder toward realistic biological membrane simulations. J Comput Chem 2014;35:1997–2004. 10.1002/jcc.23702. [PubMed: 25130509]

[36]. Lee J, Cheng X, Swails JM, Yeom MS, Eastman PK, Lemkul JA, et al. CHARMM-GUI Input Generator for NAMD, GROMACS, AMBER, OpenMM, and CHARMM/OpenMM Simulations Using the CHARMM36 Additive Force Field. J Chem Theory Comput 2016;12:405–13. 10.1021/acs.jctc.5b00935. [PubMed: 26631602]

[37]. Brown DA, Rose JK. Sorting of GPI-anchored proteins to glycolipid-enriched membrane subdomains during transport to the apical cell surface. Cell 1992;68:533–44. 10.1016/0092-8674(92)90189-J. [PubMed: 1531449]

[38]. Fujimura Y, Yamada K, Tachibana H. A lipid raft-associated 67 kDa laminin receptor mediates suppressive effect of epigallocatechin-3-O-gallate on FcεRI expression. Biochem Biophys Res Commun 2005;336:674–81. 10.1016/j.bbrc.2005.08.146. [PubMed: 16140266]

[39]. Humphrey W, Dalke A, Schulten K. VMD: Visual molecular dynamics. J Mol Graph 1996;14:33–8. 10.1016/0263-7855(96)00018-5. [PubMed: 8744570]

[40]. Phillips JC, Braun R, Wang W, Gumbart J, Tajkhorshid E, Villa E, et al. Scalable molecular dynamics with NAMD. J Comput Chem 2005;26:1781–802. 10.1002/jcc.20289. [PubMed: 16222654]

[41]. Adelman SA, Doll JD. Generalized Langevin equation approach for atom/solid-surface scattering: General formulation for classical scattering off harmonic solids. J Chem Phys 1976;64:2375–88. 10.1063/1.432526.

[42]. Feller SE, Zhang Y, Pastor RW, Brooks BR. Constant pressure molecular dynamics simulation: The Langevin piston method. J Chem Phys 1995;103:4613–21. 10.1063/1.470648.

[43]. Ryckaert JP, Ciccotti G, Berendsen HJC. Numerical integration of the cartesian equations of motion of a system with constraints: molecular dynamics of n-alkanes. J Comput Phys 1977;23:327–41. 10.1016/0021-9991(77)90098-5.

[44]. Essmann U, Perera L, Berkowitz ML, Darden T, Lee H, Pedersen LG. A smooth particle mesh Ewald method. J Chem Phys 1995;103:8577–93. 10.1063/1.470117.

[45]. Vanommeslaeghe K, Hatcher E, Acharya C, Kundu S, Zhong S, Shim J, et al. CHARMM general force field: A force field for drug-like molecules compatible with the CHARMM all-atom additive biological force fields. J Comput Chem 2010;31:671–90. 10.1002/jcc.21367. [PubMed: 19575467]

[46]. Klauda JB, Venable RM, Freites JA, O'Connor JW, Tobias DJ, Mondragon-Ramirez C, et al. Update of the CHARMM All-Atom Additive Force Field for Lipids: Validation on Six Lipid Types. J Phys Chem B 2010;114:7830–43. 10.1021/jp101759q. [PubMed: 20496934]

Author Manuscript Author Manuscript Author Manuscript Author Manuscript

[47]. Digiacomo V, Meruelo D. Looking into laminin receptor: Critical discussion regarding the non-integrin 37/67-kDa laminin receptor/RPSA protein. Biol Rev 2016;91:288–310. 10.1111/brv.12170. [PubMed: 25630983]

[48]. Stocker A Molecular mechanisms of vitamin E transport. Ann N Y Acad Sci 2004;1031:44–59. 10.1196/annals.1331.005. [PubMed: 15753133]

[49]. Min KC, Kovall RA, Hendrickson WA. Crystal structure of human α-tocopherol transfer protein bound to its ligand: Implications for ataxia with vitamin E deficiency. Proc Natl Acad Sci U S A 2003;100:14713–8. 10.1073/pnas.2136684100. [PubMed: 14657365]

[50]. Fujimura Y, Sumida M, Sugihara K, Tsukamoto S, Yamada K, Tachibana H. Green tea polyphenol EGCG sensing motif on the 67-kDa laminin receptor. PLoS One 2012;7. 10.1371/journal.pone.0037942.

[51]. Jamieson K V, Wu J, Hubbard SR, Meruelo D. Crystal structure of the human laminin receptor precursor. J Biol Chem 2008;283:3002–5. 10.1074/jbc.C700206200. [PubMed: 18063583]

[52]. Lim SW, Loh HS, Ting KN, Bradshaw TD, Zeenathul NA. Cytotoxicity and apoptotic activities of alpha-, gamma- and delta-tocotrienol isomers on human cancer cells. BMC Complement Altern Med 2014;14. 10.1186/1472-6882-14-469.

[53]. Campbell SE, Stone WL, Lee S, Whaley S, Yang H, Qui M, et al. Comparative effects of RRR-alpha- and RRR-gamma-tocopherol on proliferation and apoptosis in human colon cancer cell lines. BMC Cancer 2006;6:1–14. 10.1186/1471-2407-6-13. [PubMed: 16390557]

[54]. Yang CS, Li G, Yang Z, Guan F, Chen A, Ju J. Cancer prevention by tocopherols and tea polyphenols. Cancer Lett 2013;334:79–85. 10.1016/j.canlet.2013.01.051. [PubMed: 23403075]

[55]. Malafa MP, Neitzel LT. Vitamin E succinate promotes breast cancer tumor dormancy. J Surg Res 2000;93:163–70. 10.1006/jsre.2000.5948. [PubMed: 10945959]

[56]. Weber T, Lu M, Andera L, Lahm H, Gellert N, Fariss MW, et al. Vitamin E succinate is a potent novel antineoplastic agent with high selectivity and cooperativity with tumor necrosis factorrelated apoptosis-inducing ligand (Apo2 ligand) in vivo. Clin Cancer Res 2002;8:863–9. [PubMed: 11895920]

[57]. Davis S, Davis BM, Richens JL, Vere KA, Petrov PG, Winlove CP, et al. α - Tocopherols modify the membrane dipole potential leading to modulation of ligand bindingby P-glycoprotein. J Lipid Res 2015;56:1543–50. 10.1194/jlr.M059519. [PubMed: 26026069]

[58]. Lemaire-Ewing S, Monier S, Pais de Barros J-P, Néel D, Athias A, Royer M-C, et al. 7-Ketocholesterol Incorporation into Sphingolipid/Cholesterol-enriched (Lipid Raft) Domains Is Impaired by Vitamin E. J Biol Chem 2009;284:15826–34. 10.1074/jbc.m808641200. [PubMed: 19351882]

[59]. Tsukamoto S, Huang Y, Umeda D, Yamada S, Yamashita S, Kumazoe M, et al. 67-kDa laminin receptor-dependent Protein Phosphatase 2A (PP2A) activation elicits melanoma-specific antitumor activity overcoming drug resistance. J Biol Chem 2014;289:32671–81. 10.1074/jbc.M114.604983. [PubMed: 25294877]

[60]. Boscoboinik D, Szewczyk A, Hensey C, Azzi A. Inhibition of cell proliferation by α-tocopherol: Role of protein kinase C. J Biol Chem 1991;266:6188–94. 10.1016/s0021-9258(18)38102-x. [PubMed: 2007576]

[61]. Topham MK, Prescott SM. Mammalian diacylglycerol kinases, a family of lipid kinases with signaling functions. J Biol Chem 1999;274:11447–50. 10.1074/jbc.274.17.11447. [PubMed: 10206945]

[62]. O'Byrne D, Grundy S, Packer L, Devaraj S, Baldenius K, Hoppe PP, et al. STUDIES OF LDL OXIDATION FOLLOWING a-, g-, OR d-TOCOTRIENYL ACETATE SUPPLEMENTATION OF HYPERCHOLESTEROLEMIC HUMANS. Radiat Oncol 1990;29:371–5.

[63]. Lee MJ, Wang ZY, Li H, Chen L, Sun Y, Gobbo S, et al. Analysis of Plasma and Urinary Tea Polyphenols in Human Subjects. Cancer Epidemiol Biomarkers Prev 1995.

[64]. Morley S, Panagabko C, Shineman D, Mani B, Stocker A, Atkinson J, et al. Molecular Determinants of Heritable Vitamin E Deficiency. Biochemistry 2004;43:4143–9. 10.1021/bi0363073. [PubMed: 15065857]

[65]. Kayden HJ, Traber MG. Absorption, lipoprotein transport, and regulation of plasma concentrations of vitamin E in humans. J Lipid Res 1993. 10.1016/s0022-2275(20)40727-8.

Author Manuscript Author Manuscript Author Manuscript Author Manuscript

[66]. Hayashi D, Ueda S, Yamanoue M, Ashida H, Shirai Y. Amelioration of diabetic nephropathy by oral administration of d-α-Tocopherol and its mechanisms. Biosci Biotechnol Biochem 2018;82:65–73. 10.1080/09168451.2017.1411184. [PubMed: 29297254]

[67]. Virtamo J Incidence of Cancer and Mortality Following α-Tocopherol and β-Carotene Supplementation: A Postintervention Follow-up. J Am Med Assoc 2003;290:476–85. 10.1001/jama.290.4.476.

[68]. Lippman SM, Klein EA, Goodman PJ, Lucia MS, Thompson IM, Ford LG, et al. Effect of Selenium and Vitamin E on Risk of Prostate Cancer and Other Cancers. Jama 2009;301:39. 10.1001/jama.2008.864. [PubMed: 19066370]

[69]. Butò S, Tagliabue E, Ardini E, Magnifico A, Ghirelli C, Van Den Brûle F, et al. Formation of the 67-kDa laminin receptor by acylation of the precursor. J Cell Biochem 1998;69:244–51. [PubMed: 9581863]

[70]. Castronovo V, Taraboletti G, Sobel ME. Functional domains of the 67-kDa laminin receptor precursor. J Biol Chem 1991;266:20440–6. [PubMed: 1834645]

[71]. Fujimura Y, Umeda D, Yamada K, Tachibana H. The impact of the 67 kDa laminin receptor on both cell-surface binding and anti-allergic action of tea catechins. Arch Biochem Biophys 2008;476:133–8. 10.1016/j.abb.2008.03.002. [PubMed: 18358230]

Author Manuscript Author Manuscript Author Manuscript Author Manuscript

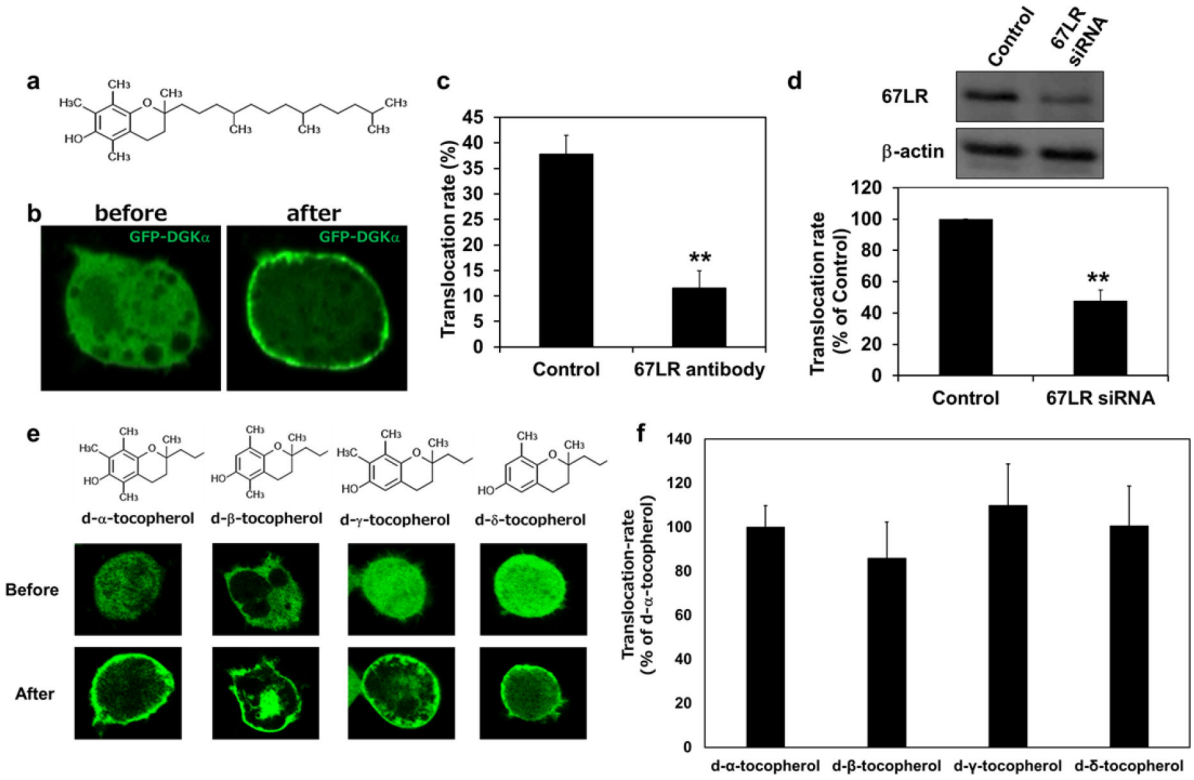

Fig. 1. Translocation of DGKα to the plasma membrane induced by tocopherols.

(a) Structure of αToc. **(b)** Localization of GFP-DGKα in DDT1-MF-2 cells before and 3 minutes after 200 μM αToc stimulation. **(c)** The translocation rate of GFP-DGKα in DDT1-MF-2 cells by 200 μM αToc in the absence or presence of anti-67LR antibody treatment. *N*=4. **(d)** Effect of the knockdown of 67LR on the translocation of GFP-DGKα in DDT1-MF-2 cells by 200 μM αToc. *N*=3. **(e)** Localization of GFP-DGKα in DDT1-MF-2 cells before and 3 minutes after 200 μM tocopherol stimulation. The difference in the position of the methyl moiety in the structure of each of the tocopherols is shown above the respective pictures. **(f)** The translocation rate of GFP-DGKα in DDT1-MF-2 cells induced by each of the tocopherols. *N*=3. The data shows the percentage of the translocation rate relative to αToc. The values are mean ±SE. Asterisks indicate significance (**$p < 0.01$). Full-length blots are presented in Fig. S1.

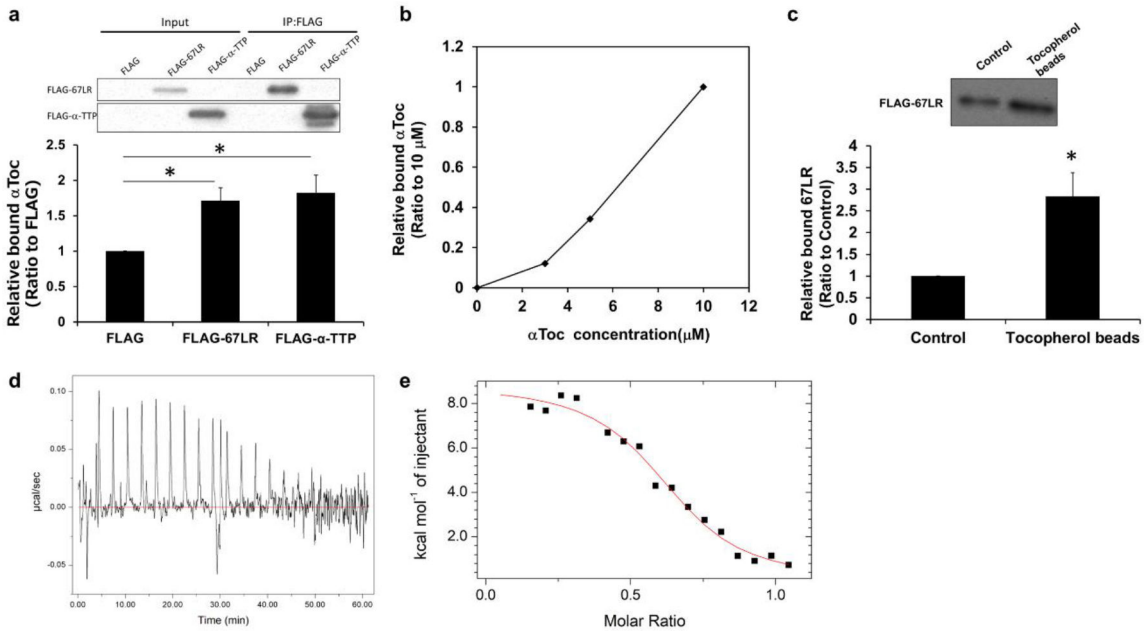

Fig. 2. Direct binding between αToc and 67LR and its affinity.

(a) The result of the binding assay between 10 μM αToc and precipitated FLAG-67LR or FLAG-α-TTP using HPLC is shown. The expression and precipitation of FLAG-67LR and FLAG-α-TTP were detected by western blot. The value is the ratio of bound αToc to FLAG alone. *N*=4. **(b)** Concentration-dependent binding of αToc to 67LR detected by the binding assay using HPLC. The value was shown as a percentage of 10 μM. **(c)** The result of the binding assay using tocopherol conjugated beads. The amount of precipitated FLAG-67LR by the control and tocopherol conjugated beads was detected by western blot. **(d)** The representative raw data of ITC for titration of 120 μM GST-67LR-His to 20 μM αToc at 298K. **(e)** The integrated area under the curve of each peak from **(d)** was plotted by the molar ratio of GST-67LR-His and αToc. The best fit curve was drawn by the Origin software, and the K_d value was calculated based on the curve. The intensity of bands in the western blots were analyzed by Image J. The error bars show SE. Asterisks indicate significance (*$p < 0.05$). Full-length blots are presented in Fig. S2 and S4.

Author Manuscript Author Manuscript Author Manuscript Author Manuscript

Author Manuscript Author Manuscript Author Manuscript Author Manuscript

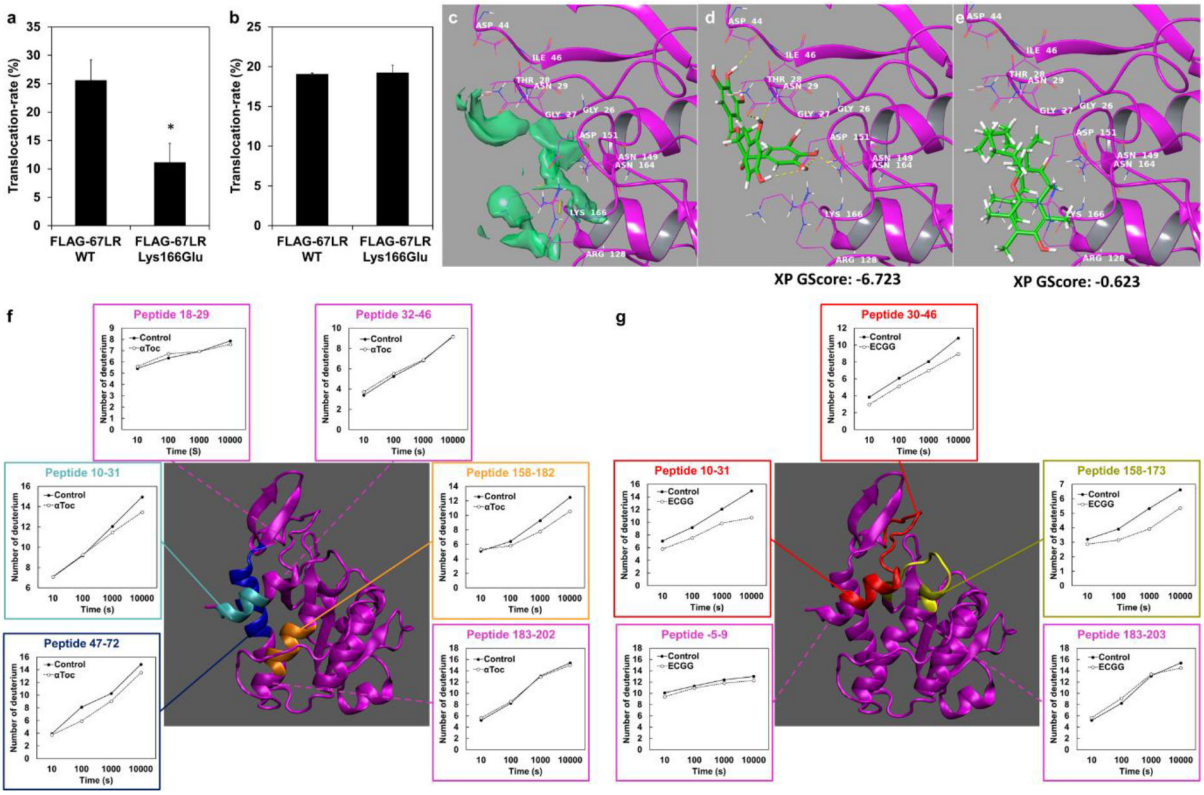

Fig. 3. The putative αToc binding site on 67LR determined by HDX/MS.

The effect of overexpression of FLAG-67LR Lys166Glu on 200 μM **(a)** EGCG or **(b)** αToc-induced translocation of GFP-DGKα in DDT1-MF-2 cells. *N*=3 **(c)** The image of the EGCG binding site of 67LR (green: hydrophilic surface). The docking simulations of **(d)** EGCG and **(e)** αToc to the putative EGCG binding site of 67LR by Glide software. Hydrogen bonds are shown as a yellow dashed line. **(f)** The change in the number of deuterium in the typical reproduced regions by αToc (Cyan: Lys11-Lys17, Blue: Asn50-Ala61, Orange: Trp176-Leu183). **(g)** The change in the number of deuterium in the typical reproduced regions by EGCG (Red: Leu16-Met34, Yellow: Ile161-Gly172). The dashed lines point the residues neighboring color-coded residues show no significant difference in number of deuterium. The amino acid sequence includes the remaining N-terminal linker to the GST tag and the C-terminal 6×His tag. The error bars show SE. Asterisks indicate significance (*$p < 0.05$).

Author Manuscript Author Manuscript Author Manuscript Author Manuscript

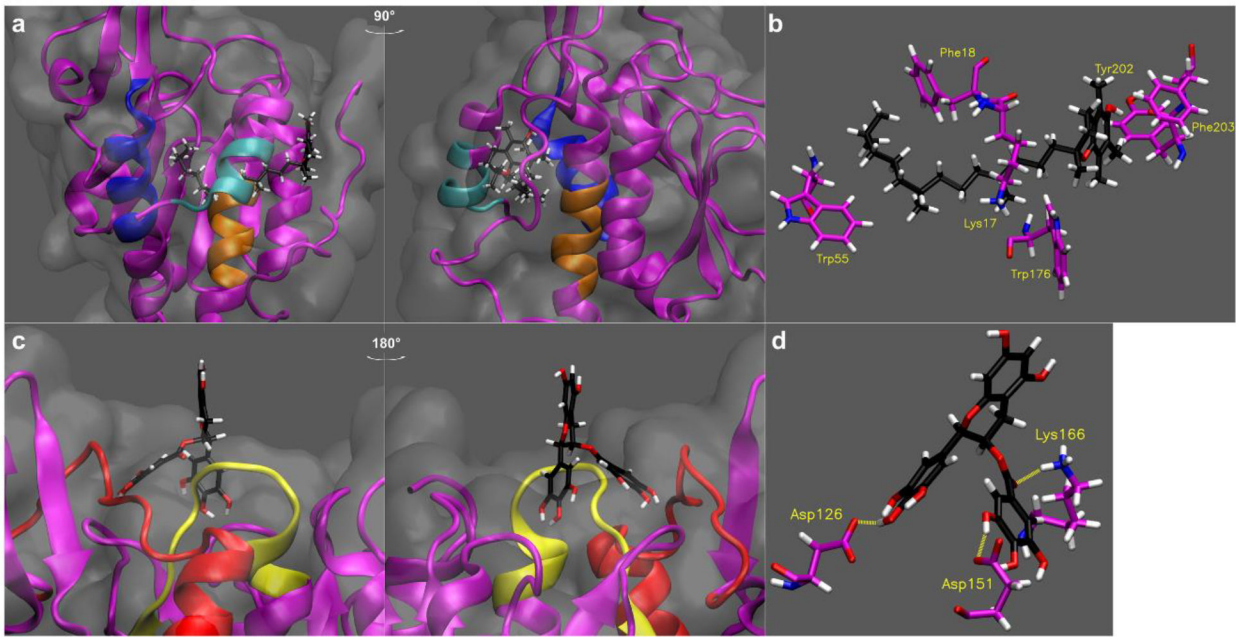

Fig. 4. Binding simulations of αToc and EGCG to their respective putative binding sites.

The binding mode of **(a)** αToc and **(c)** EGCG in 67LR (the final frame of the simulations shown in Movie S1 and S3). The typical amino acid residues in the binding mode of **(b)** αToc and **(d)** EGCG in 67LR. The structure of αToc and EGCG are shown in black, and the colored regions are the same as shown in Fig. 3, respectively. The surface of the protein was shown in a gray transparent cloud. The hydrogen bonds are shown as a yellow dashed line (distance cutoff: 3.2Å, angle cutoff: 30°).

Author Manuscript Author Manuscript Author Manuscript Author Manuscript

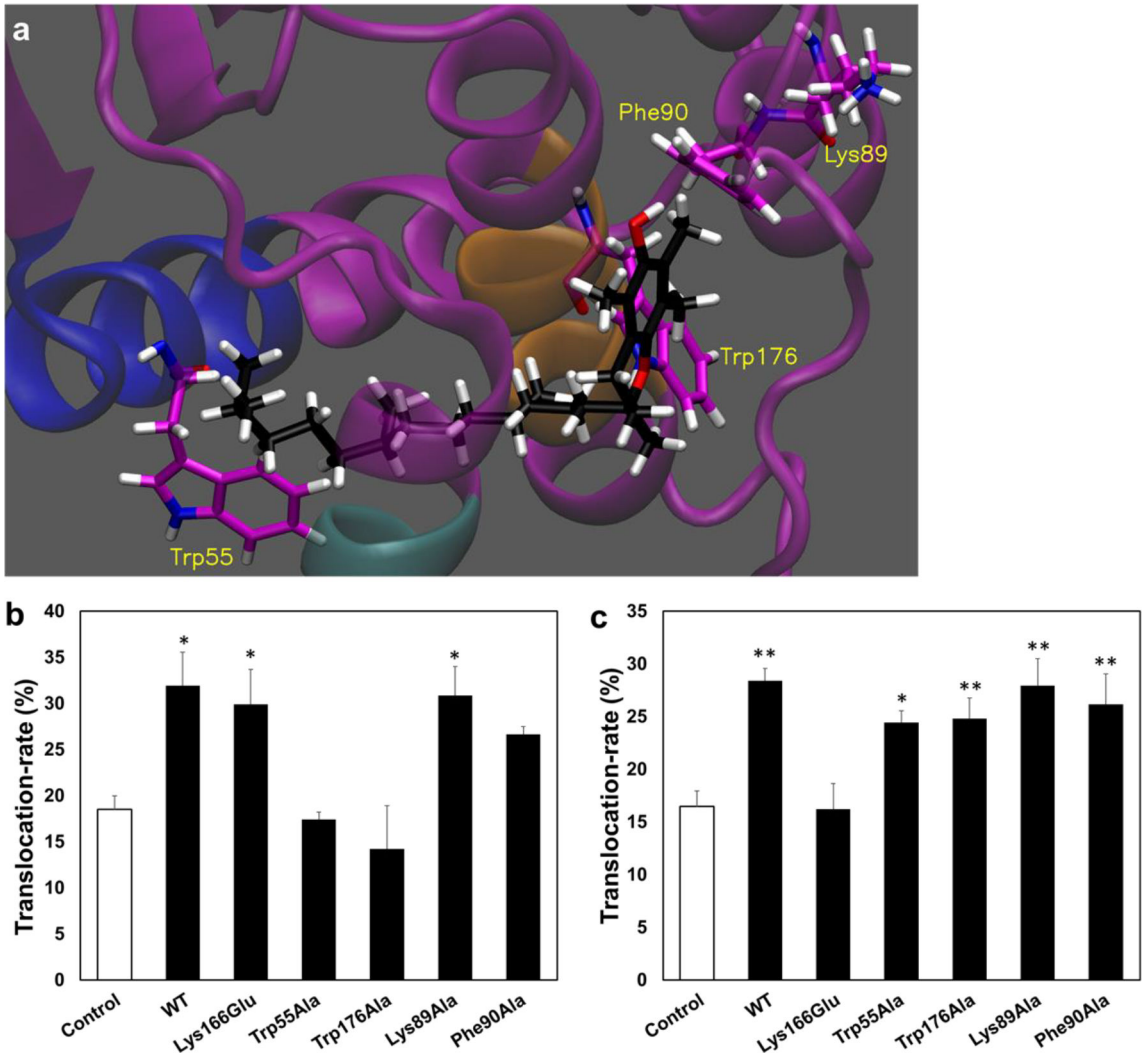

Fig. 5. The effect of mutants in the αToc binding site on the translocation of DGKα.

(a) The position of mutated amino acids in the αToc binding region is shown. The effect of overexpression of the mutants on the 200 μM **(b)** αToc (*N*=3) or **(c)** EGCG (*N*=3) -induced translocation of GFP-DGKα in DDT1-MF-2 cells. The Control is the overexpressed FLAG vector alone in the cells. The error bars show SE. Asterisks indicate significance comparing to Control (*$p < 0.05$, **$p < 0.01$).

Author Manuscript Author Manuscript Author Manuscript Author Manuscript

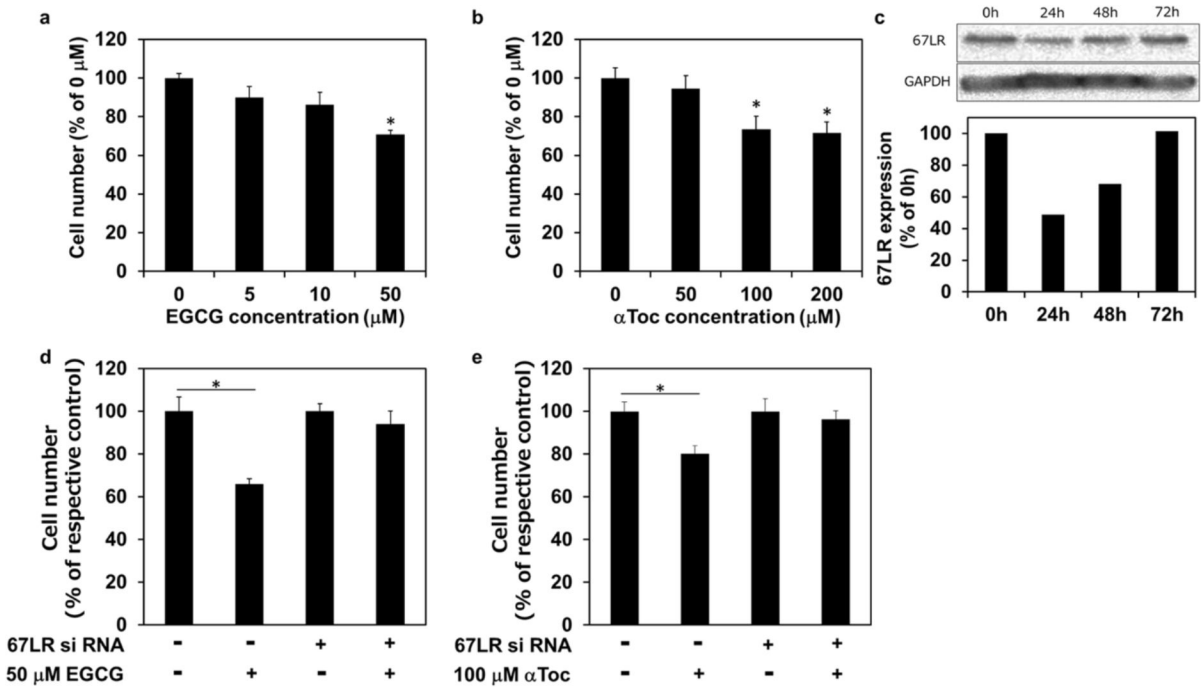

Fig. 6. Effect of the knockdown of 67LR on the anticancer effect of EGCG and αToc.

The effects of various concentrations of **(a)** EGCG (*N*=3) or **(b)** αToc (*N*=3) on the viability of HCT116 cells. The value is shown as a percentage of that seen with no addition (0 μM). **(c)** Changes in the expression of 67LR after siRNA transfection. The effects of the knockdown of 67LR on the **(d)** 50 μM EGCG (*N*=3) or **(e)** 100 μM αToc (*N*=3) -induced decrease of HCT116 cell viability. The error bars show SE. Asterisks indicate significance comparing to respective control (*$p < 0.05$).

Author Manuscript Author Manuscript Author Manuscript Author Manuscript

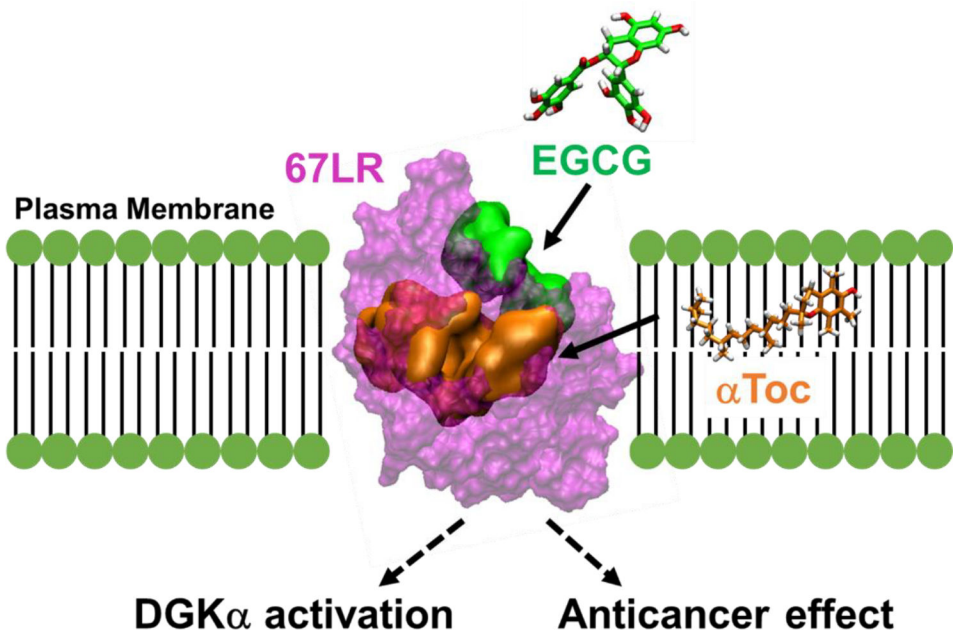

Fig. 7. Model for the EGCG and αToc binding sites on 67LR and its functions.

The transparent purple surface shows the entire 67LR. The green surface shows a hydrophilic EGCG binding site facing the outer environment. The orange surface shows a hydrophobic αToc binding site embedded in the membrane.